이학석사 학위논문

Microphysical Properties of Arctic Clouds: 2-year Ground-Based Remote Sensing Observations at Ny-Ålesund, Svalbard

니알슨 지역 지상 원격 관측자료를 활용한 북극 구름의 미세물리 특성 연구

2020년 8월

서울대학교 대학원

지구환경과학부

조 연 수

Abstract

Geometrical (cloud fraction and cloud height) and microphysical (liquid water content; LWC, ice water content; IWC, and effective radius; R_{eff}) properties of Arctic clouds were investigated using ground-based remote sensing observations (cloud radar, ceilometer, and microwave radiometer) from June 2016 to May 2018 at Ny-Ålesund (78.92 °N, 11.93 °E), Svalbard. This study analyzed the monthly variation of cloud properties depending on cloud type (liquid, ice, and mixed-phase clouds) and evaluated their relationship with air masses advection. The total cloud fraction at Ny-Ålesund was 78 % during the study period, and ice clouds (47 %) were most frequent. Concerning cloud fraction and LWC/IWC, the values of liquid clouds and ice clouds were higher in summer/fall and winter/spring, respectively. Those of mixed-phase clouds, on the other hand, did not show a distinct monthly variation. The influences of warm and cold advection on cloud microphysical properties were identified focusing on winter. Results showed that low-level mixed-phase clouds were more than two times frequent, and LWC/IWC also increased an order of magnitude under warm advection transported from the North Atlantic Ocean. Furthermore, cloud microphysical properties influenced by warm advection contributed to a downward

longwave cloud radiative effect (LW CRE) which was 145 W m^{-2} higher than cold advection, resulting in warming of the surface.

Key Words: Arctic clouds, Ground-based remote-sensing observation, Cloud microphysical properties, Advection, Longwave cloud radiative effect

Student Number: 2018-27016

Table of Contents

List of Tables

List of Figures

Chapter 1. Introduction

1.1 Background

Arctic clouds play important roles in the energy budget. They scatter shortwave (SW) radiation and emit longwave (LW) radiation, resulting in cooling and warming the surface, respectively (Goosse et al., 2018). Since the Arctic has low humidity in the atmosphere and snow and ice on the surface, the region has been discussed as a sensitive region to radiative effects (Serreze et al., 2009). The relationship between clouds and radiation is described in a complex cloud-radiation feedback mechanism, and cloud properties are significant factors that lead the mechanism (Curry et al., 1996). The influence of both geometrical (cloud fraction, height, and thickness) and microphysical properties (cloud phase, water content, size, and shape) of clouds on the surface radiation budget have been identified by previous researches (Shupe et al., 2004; Dong et al., 2010; Ebell et al., 2020). It is necessary to precisely characterize Arctic clouds for a better understanding of the Arctic climate and the enhanced prediction of global climate change.

Diverse measurements have been implemented from the space and the surface to investigate these cloud properties. The vertical and

seasonal variation of Arctic clouds were analyzed from the Cloud-Aerosol Lidar and Infrared Pathfinder (CALIPSO) and CloudSat (Mioche et al., 2015; Liu et al., 2017). Ship-based and ground-based observations were also performed at six sites in the Arctic (Shupe et al., 2011a, b). Compared to space-borne observations, ground-based observations were able to more accurately capture low-level clouds, which were most common in the Arctic (Blanchard et al., 2014; Liu et al., 2017). Accordingly, observatories have been organized at many sites in the Arctic, one of which is Ny-Ålesund. Although clouds have been observed at this site for a long time, they were limited to cloud base height measurements until recently (Maturilli and Ebell, 2018; Yeo et al., 2018). Thus, to improve the understanding of the vertical cloud structure, Nomokonova et al. (2019), for the first time, tried to use the synergy of radar-lidar. They succeeded to analyze the vertical distribution of clouds at Ny-Ålesund. Nevertheless, cloud microphysical properties still require further studies of their vertical and seasonal variation.

Ny-Ålesund (78.92 °N, 11.93 °E) is an interesting region where warm and cold air masses intersect. The region is located on the west coastline of Svalbard between the Greenland Sea and the Barents Sea, and it is the warmest part of the Arctic due to its surrounding warm ocean (Serreze et al., 2011). Low sea ice extents are observed in the vicinity of

the site. The large open ocean enables warm and moist air masses to be transported by south/southwesterly winds into Ny-Ålesund (Maturilli and Kayser, 2017), and they meet cold and dry air masses from the central Arctic transported by northerly winds. These air circulations affect cloud formation and properties, which can contribute to the surface radiation budget. There are many studies on the relationship between the radiative effects of clouds and circulation in this area (Mioche et al., 2015; Yeo et al., 2018; Kim et al., 2017; Yamanouchi, 2019). However, little research focused on the quantitative variation of cloud microphysical properties by circulation.

1.2 Objectives of this study

This study aims to investigate the monthly variation of geometrical and microphysical properties of three different cloud types at Ny-Ålesund and to evaluate the effects of air mass origin on the cloud microphysical properties and LW radiation. Details are as follows:

(1) Investigating the geometrical and microphysical cloud properties over Ny-Ålesund, Svalbard.

- To classify the cloud types into liquid, ice, and mixed-phase clouds.

- To examine the monthly variation of geometrical cloud properties such as cloud fraction and cloud height, and microphysical cloud properties such as liquid water content, ice water content, and effective radius.

(2) Evaluating the influences of atmospheric circulation on the cloud microphysical properties in winter.

- To identify the relationship between air mass origin and cloud microphysical properties.

- To investigate the effects of circulation on surface LW cloud radiative effect.

Chapter 2. Methodology

2.1 Measurements

Three ground-based remote sensing instruments, cloud radar, ceilometer, and microwave radiometer, were used to investigate the cloud properties at Ny-Ålesund, Svalbard. Table 1 summarizes the technical specifications and parameters derived from these instruments. All three instruments have been continuously operated at the AWIPEV observatory by the Alfred Wegener Institute Helmholtz Centre for Polar and Marine Research (AWI) and the French Polar Institute Paul Emile Victor (PEV). Within the Transregional Collaborative Research Center (TR 172) project "Arctic Amplification: Climate Relevant Atmospheric and Surface Processes, and Feedback Mechanisms (AC3)", the observations have been made since June 2016 (Nomokonova et al., 2019). It is the first simultaneous observations of three ground-based remote sensing instruments to examine the cloud vertical structure at Ny-Ålesund.

A 94GHz cloud radar (model: JOYRAD-94) was installed by the University of Cologne, described in detail by Küchler et al. (2017). The ceilometer (model: Vaisala CL51) emits 905 nm light to derive the

Table 1. Technical specifications and derived quantities of ground-based remote sensing instruments.

	FMCW 94 GHz Cloud Doppler Radar (model: JOYRAD-94)	Ceilometer (model: Vaisala CL51)	Microwave Radiometer (model: HATPRO)
Wavelength	94 GHz	905 nm	K-band (22.24 – 31.40 GHz) V-band (51.26 – 58.00 GHz)
Derived products	Reflectivity factor (Z) Doppler-velocity Doppler Spectral Width	Attenuated backscatter coefficient (β)	Brightness temperature
Reference	Küchler et al. (2017)	Maturilli and Ebell (2018)	Rose et al. (2005)

attenuated backscatter coefficient (β; Maturilli and Ebell, 2018). By using the synergy of cloud radar and ceilometer, we can get information on the cloud vertical structure. Cloud radar is more sensitive to large particles such as rain, drizzle drops, and ice particles, while the ceilometer detects smaller particles such as cloud droplets and aerosols. From the difference of principle, clouds at the upper level can also be detected. The microwave radiometer (MWR; model: HATPRO) has been operated since 2011 (Rose et al., 2005). It is utilized to retrieval the liquid water path

(LWP), integrated water vapor (IWV), and temperature profiles by measuring the brightness temperature at K-band (22.24 – 31.40 GHz) and V-band (51.26 – 58.00 GHz).

2.2 Data analysis

The synergy of ground-based remote sensing observations can provide the estimates (Cloudnet; Illingworth et al., 2007) of cloud properties such as phase, liquid water content (LWC), ice water content (IWC), and effective radius (R_{eff}) combined with thermodynamic properties from a numerical weather prediction (NWP) model, such as GDAS1 or NWP ICON. One of the essential datasets used in this study is the target classification product, information on the phase of each bin in vertical profiles (Hogan and O'Connor, 2004). The resolution of a bin is 30 seconds in time and 20 meters in the vertical. Radar reflectivity factor (Z) and ceilometer β profiles are used to detect the presence and position of clouds. To distinguish phase, additional parameters such as temperature, wet bulb temperature, and doppler velocity are utilized. In the end, it defines the phase of each bin as one of the 11 kinds of phase; (1) clear-sky, (2) cloud droplets, (3) drizzle or rain, (4) drizzle/rain and cloud droplets, (5) ice, (6) ice and supercooled droplets, (7) melting ice,

(8) melting and cloud droplets, (9) aerosol, (10) insects, and (11) aerosol and insects.

Microphysical properties of clouds are also derived by applying the empirical equations from previous studies, based on the target classification. Detailed retrieval algorithms are summarized in Table 2. LWC was calculated by scaled adiabatic method for the profiles where the liquid phase was detected, and LWP measured from MWR was available. Combining with LWP, model temperature (T) and pressure were also used to retrieve theoretical adiabatic LWC. The vertical integrated LWC should match the LWP. On the contrary, if the ice phase was present, IWC was retrieved by empirical formula from Hogan et al. (2006) using Z and T. Moreover, the retrieved R_{eff} of cloud droplets was based on the equation from Frisch et al. (2002). Both Z and LWP were utilized as input variables, and cloud droplet concentration was assumed to be 74 cm^{-3} (Miles et al., 2000). The R_{eff} of ice particles was calculated following equation with IWC and visible extinction coefficient (α; Hogan et al., 2006), which were functions of both Z and T (Delanoë et al, 2007). Note that IWC and R_{eff} of ice particles may be overestimated because the target classification does not discriminate between snow and cloud ice.

Table 2. Retrieval methods of cloud microphysical properties.

Parameters	Equations	Reference
Liquid Water Content (LWC)	Scaled adiabatic method using LWP from MWR	
Ice Water Content (IWC)	$\log_{10}(IWC)$ = (0.00058) ZT + (0.0923) Z − (0.00706) T − 0.992 (Z = Z [measured] x 0.7194)	Hogan et al. (2006)
Effective Radius (Liquid)	$r_e(h) = \frac{Z^{\frac{1}{6}}(h)}{2Q^{\frac{1}{3}}}\left(\frac{\pi\rho}{6}\right)^{\frac{1}{3}}\left(\sum_{i=1}^{i=m} Z^{\frac{1}{2}}(h_i)\Delta h\right)^{\frac{1}{3}} \exp(-2\sigma_x^2)$ Z = Radar reflectivity factor H_i = Height in the cloud i (0 – m) = Radar range gate at cloud base and cloud top Δh = Radar range gate thickness ρ = Water density Q = Integrated liquid water through the depth of the cloud (LWP) σ_x = Logarithmic spread of the distribution (assume 0.38)	Frisch et al. (2002)
Effective Radius (Ice)	$r_e = \frac{3(IWC)}{2\rho_i\alpha}\,10^6$ (ρ_i = Solid ice density; 0.917 g cm^{-3}) $\log_{10}(\alpha) = (0.000876)ZT + 0.0928Z - (0.00513) - 2.49$	Delanoë et al. (2007)

The identification of the clouds followed the method used by Nomokonova et al. (2019). To identify cloud layers, all the target classification profiles from Cloudnet were checked. If more than three consecutive bins in a vertical profile had liquid or ice, it was considered a cloud layer. Depending on the phase of bins existing in an identified cloud layer, its cloud type was decided; liquid, ice, and mixed-phase clouds. Liquid clouds and ice clouds were defined if only one single phase, liquid or ice, was present within the cloud layers. On the other hand, cloud layers were considered as mixed-phase clouds if both liquid and ice phases were contained within the same cloud boundary. Note that both phases did not need to be present in the same bin. This implies the various cloud structures of mixed-phase clouds regardless of where liquid or supercooled droplets were located within the cloud boundary. Single-layer clouds and multilayer clouds were distinguished by the number of identified cloud layers in a vertical profile. If at least one clear-sky bin was present between the cloud layers, they were identified as different cloud layers.

Chapter 3. Results and Discussion

3.1 Geometrical properties of clouds

In this section, geometrical properties of clouds were investigated using Cloudnet datasets. Here, the geometrical properties were the cloud fraction and height. Clouds were separated into three types, liquid, ice, and mixed-phase clouds with the method described in Section 2.2. Additionally, clouds can be classified into single-layer and multilayer. However, the latter is normally excluded when clouds were examined using the remote sensing observations due to large uncertainty. It is difficult to detect the second cloud layer including the liquid if the first liquid layer is already detected because the lights emitted from the ceilometer are extinguished from the lower layer. Thus, multilayer liquid clouds and mixed-phase clouds of the upper level are possibly underestimated, while ice clouds are overestimated. This study, nevertheless, contained multilayer clouds for two reasons. The first one was that their frequency (38 %) was too high to be ignored compared to that of single-layer clouds (39%). Another reason was that liquid phase of multilayer clouds, which are most susceptible to uncertainty, was not likely to be present at high altitudes due to low temperatures.

Figure 1 gives the vertical distributions of the cloud fraction for three different cloud types during the study period. To calculate the monthly mean cloud fraction at a certain altitude, bins are counted according to their classified groups and normalized by the total number of profiles for each month. The annual mean cloud fraction was obtained from the monthly-averaged values. It can be seen that total clouds occurred predominantly at altitudes lower than 2 km (Figure 1a).

Three cloud types showed distinctly different characteristics. Concerning seasonality, liquid clouds and ice clouds had a clear seasonal variation. The occurrence frequency of liquid clouds was highest in summer, while that of ice clouds was highest in winter. In the annual average vertical profile, the maximum cloud fraction of liquid and ice clouds were observed at 0.8 km and 4 – 5 km, respectively (Figures 1b and 1c). However, mixed-phase clouds had no strong seasonal variation. High cloud fraction was observed at less than 2 km throughout the year, especially during the transition months, May and October (Figure 1d). These seasonalities of clouds were associated with the air temperature variation by the seasonal cycle of solar radiation in the Arctic (polar day and polar night). In other words, the air temperature ranges in which clouds occur depend on the cloud phase (Nomokonova et al., 2019). MWR

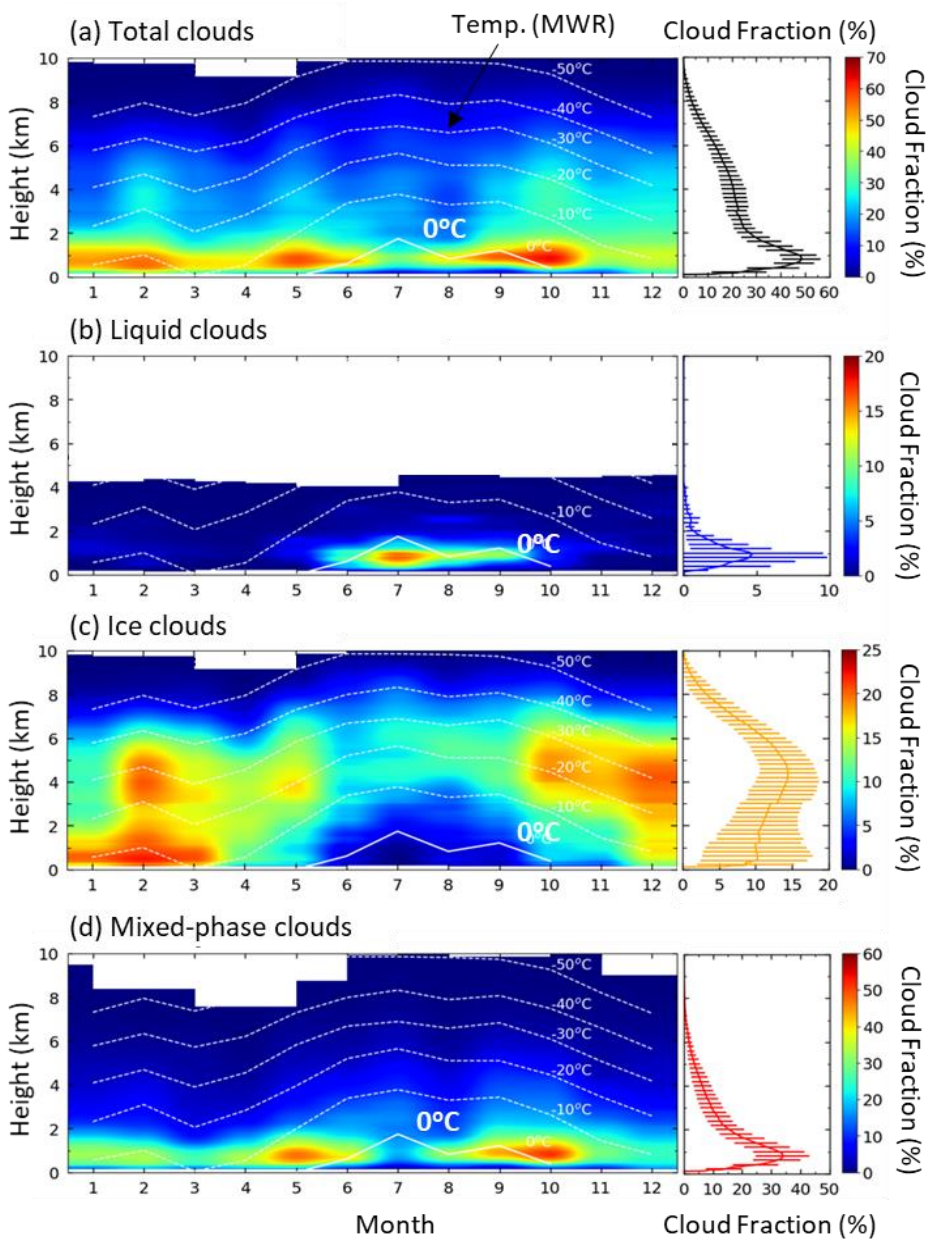

Figure 1. The monthly (left) and annual (right) mean vertical distribution of cloud fraction for (a) total clouds, (b) liquid clouds, (c) ice clouds, and (d) mixed-phase clouds from June 2016 to May 2018. The ranges of cloud fraction are different depending on cloud type. White lines indicate the isotherm with intervals of 10 °C, which are calculated by applying air temperature (MWR) into a linear interpolation method.

was used to check the relationship between the cloud phase and temperature. Since the instrument retrieved discontinuous air temperature in the vertical, continuous monthly mean values were calculated using a linear interpolation method. White isothermal lines were drawn at intervals of 10 °C on the vertical distribution of Figure 1. Liquid clouds typically occurred when the air temperature is over 0 °C, whereas the ice clouds mostly occurred at the temperature between -40 °C and -10 °C. For the mixed-phase clouds, cloud fraction was high at temperatures from -15 °C to 0 °C. Since ice particles are known to grow by deposition most efficiently in the temperature ranges from -15 °C to 5 °C (Fukuta and Takahashi, 1999), mixed-phase clouds were frequently found at these temperature conditions.

Comparison of cloud fraction between Ny-Ålesund and other regions in the Arctic (Barrow, Alaska; Surface Heat Budget of the Arctic Ocean (SHEBA); Eureka, Canada) was shown in Figure 2. In this study, clouds were observed for 78 % of the study period. It was calculated by the ratio between the number of profiles with cloud layers and the total number of profiles in the corresponding month. The most frequent type was ice clouds (47 %), followed by mixed-phase clouds (44 %), and liquid clouds (15 %). Shupe et al. (2011b) analyzed the cloud statistics at three

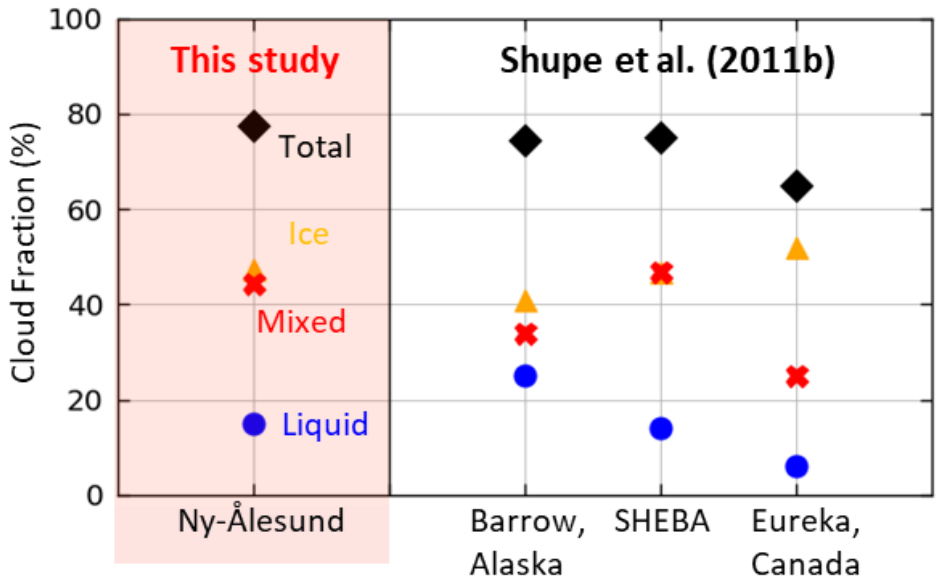

Figure 2. Comparison of annual mean cloud fraction between Ny-Ålesund (left side) and other sites in the Arctic (right side; Barrow, Alaska; SHEBA; Eureka, Canada from Shupe et al., 2011b). The symbols indicate total clouds (diamond; black), liquid clouds (circle; blue), ice clouds (triangle; yellow), and mixed-phase clouds (cross; red).

stations in the Arctic using the synergy of radar and lidar. The total cloud fraction was slightly higher in this study than other sites regardless of latitude (Figure 2), which was attributed to diabatic heating by the near warm ocean (Serreze et al., 2011). In particular, the occurrence frequency of mixed-phase clouds at Ny-Ålesund was as high as that of SHEBA, a ship-based observation. The occurrence of low-level mixed-phase clouds at Ny-Ålesund may be affected by large-scale advection (Mioche et al., 2015).

The statistics of the highest cloud top height (CTH) and the lowest cloud base height (CBH) for three cloud types are displayed in Figure 3. Among the cloud layers in a vertical profile, the highest CTH of the uppermost cloud layer was averaged as the highest top height. Likewise, the lowest CBH was calculated by using the lowermost cloud layer in a vertical profile. The highest CTH ranged from 3 to 4.5 km, and the lowest CBH ranged from 1 to 1.5 km (Figure 3a). Similar to the abovementioned cloud fraction, cloud height also changed following the monthly variation in atmospheric temperature. Both the lowest CBH and highest CTH of liquid clouds are subtly decreased in summer. The difference between the top and the base of liquid clouds was the smallest (Figure 3b). On the contrary, the average CTH and CBH of ice and mixed-phase clouds tended to increase in summer. CTH and CBH of ice clouds were highest, and CBH of mixed-phase clouds were lowest (Figures 3c and 3d).

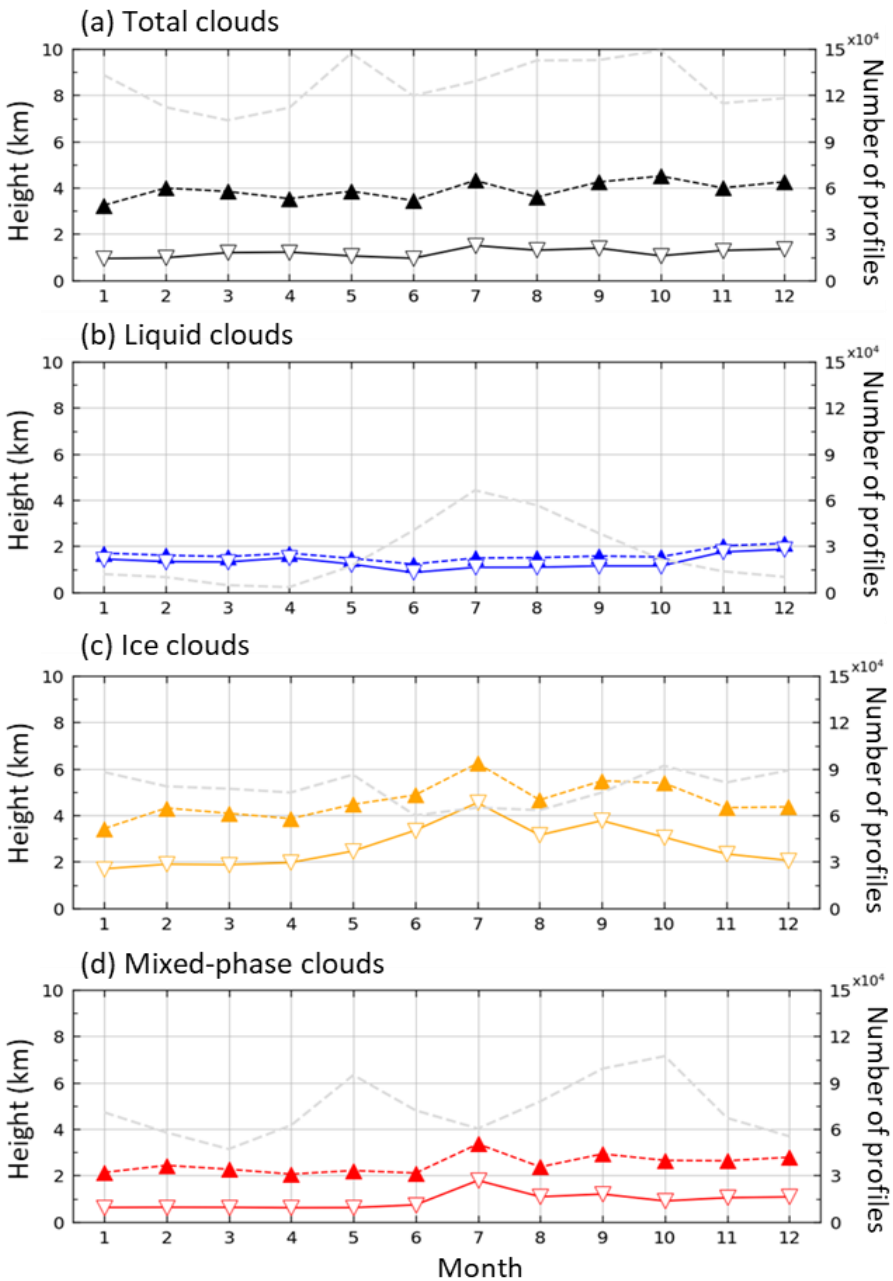

Figure 3. The monthly variation of highest cloud top height (CTH; filled triangle; dashed lines) and lowest cloud base height (CBH; opened upside-down triangle; solid lines) for (a) total clouds, (b) liquid clouds, (c) ice clouds, and (d) mixed-phase clouds during June 2016 to May 2018. The grey dashed lines indicate the monthly average number of profiles when each cloud type was present.

3.2 Microphysical properties of clouds

For three cloud types, vertical distributions of LWC and IWC were examined as one of the microphysical properties. The cloud phase and its content are important determining the radiative properties (Shupe and Intrieri, 2004). Notice that LWC and IWC were retrieved only for liquid-containing bins and ice-containing bins, respectively. Thus, mixed-phase clouds had vertical distributions of both LWC and IWC. Monthly mean values were calculated when clouds were present based on the method discussed in Section 2.2.

Figure 4 represents the monthly mean characteristics of LWC and IWC for three cloud types. LWC in liquid clouds had seasonal variation which was high at low altitudes in summer and fall (Figure 4a). That is, optically thick liquid clouds were present when solar radiation was strong. IWC in ice clouds represented opposite seasonality which had the highest values in winter, polar night (Figure 4b). In contrast, liquid and ice in mixed-phase clouds had no variation by month (Figure 4c). LWC was high at low altitudes not only in summer and fall but also in winter and spring. Likewise, IWC in mixed-phase clouds showed no explicit monthly variation (Figure 4d). The ratio of LWC to IWC in mixed-phase clouds over Ny-Ålesund was high between 1 km and 4 km altitudes,

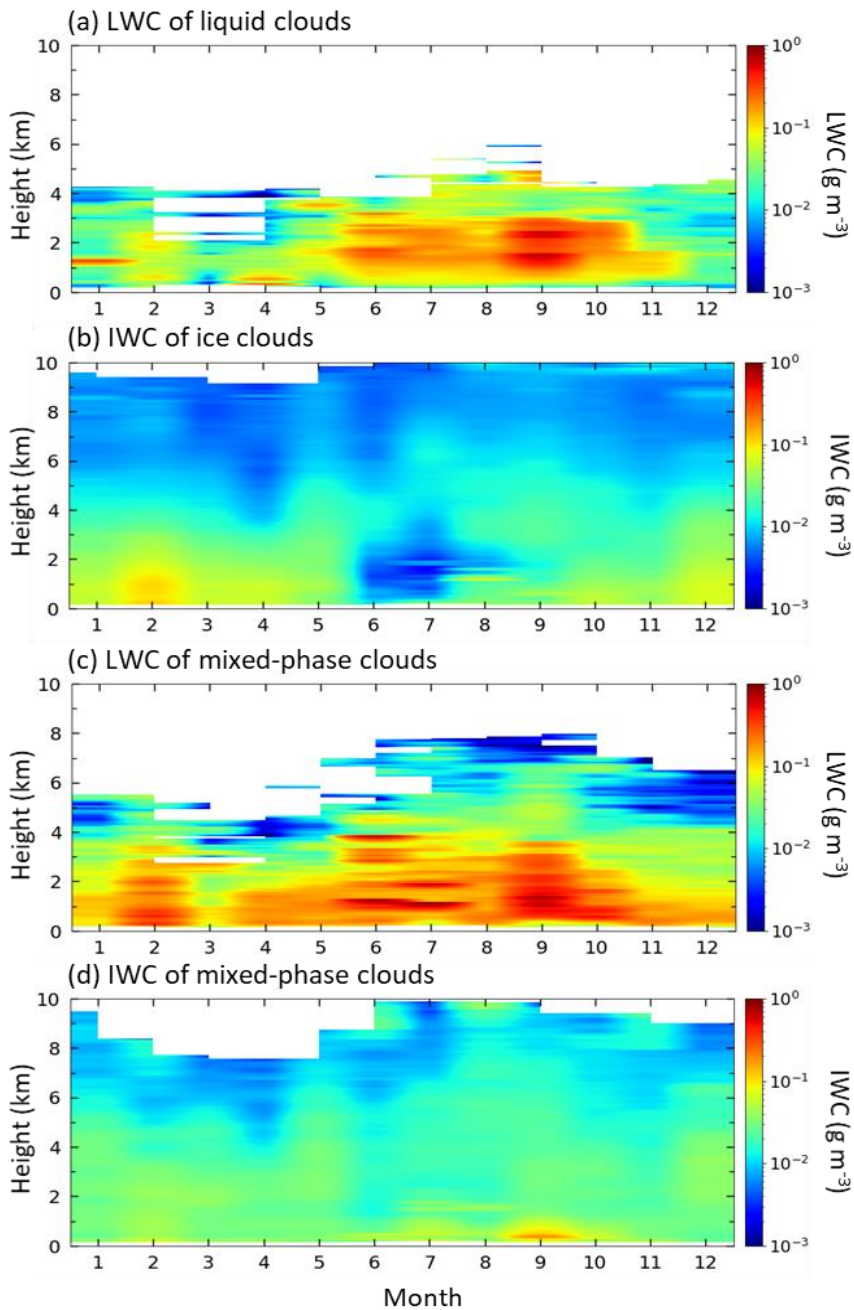

Figure 4. The monthly vertical distribution of liquid water content (LWC; g m^{-3}) for (a) liquid clouds and (c) mixed-phase clouds, and of ice water content (IWC; g m^{-3}) for (b) ice clouds and (d) mixed-phase clouds from June 2016 to May 2018. The ranges of values are represented by a log-scale color bar.

particularly in summer and fall. As the amount of liquid water, rather than ice water, in clouds was an important contributor to the Arctic surface radiation budget, the ratio of LWC to IWC is an important factor for evaluating the radiative effects of mixed-phase clouds (Shupe and Intrieri, 2004).

LWC and IWC in mixed-phase clouds at Ny-Ålesund are compared to results from other regions in the Arctic (Figure 5). Shupe et al. (2005) showed annual mean LWP and IWC derived from ground-based remote sensing sensors at SHEBA. Boer et al. (2009) analyzed averaged LWP and IWC during fall in Barrow and Eureka. Water contents were different depending on the region. Ny-Ålesund had almost similar annual mean LWP and IWC compared to SHEBA, which was a ship-based observation campaign operated at 75 – 80 °N latitudes. Moreover, clouds at Ny-Ålesund were more than twice as high in water content from those at Eureka (80.00 °N, 85.57 °W) during the fall season despite the slightly lower latitude. This suggests that, in addition to the occurrence of low-level mixed-phase clouds, LWC and IWC can also be influenced by atmospheric circulation (Mioche et al., 2015; Gierens et al., 2020). Relatively high values of LWC and IWC in September were also associated with large-scale advection (Figure 4). Considering geopotential height at 850 hPa by ERA5 reanalysis data during the study period, results

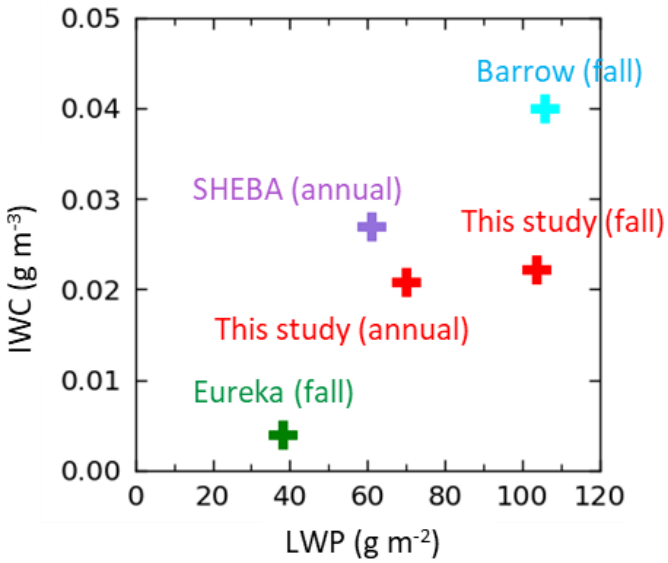

Figure 5. Comparison of IWC (g m^{-3}) and LWP (g m^{-2}) between Ny-Ålesund (this study; red) and other sites (Barrow, Alaska; blue, SHEBA; purple, Eureka, Canada; green).

revealed that transports from the North Atlantic Ocean by south-westerly winds were dominant in September (not shown).

The droplet size distribution may also alter the optical properties of clouds resulting in sufficiently changes of the global energy budget (Twomey, 1977). Note that R_{eff} for cloud droplets was calculated only for single-layer liquid clouds, while R_{eff} for ice particles was obtained for both ice and mixed-phase clouds. Outliers were removed to increase the statistical reliability. They correspond to data points higher than 1.5 interquartile range (IQR) above the third quartile and lower than 1.5 IQR below the first quartile.

Figure 6 shows the monthly vertical distribution and median values of R_{eff} for liquid droplets and ice particles. Droplets in single-layer liquid clouds seem to increase by height in winter and spring (Figure 6a, bottom). This can be the result of low LWC and a shortage of data. There was little difference in monthly variation of ice particles between ice and mixed-phase clouds (Figures 6b and 6c, bottom); Ice particles were larger at low altitudes in summer and fall than other seasons. High values in summer reflect the growth of ice by aggregation at increased temperature (Shupe et al., 2005), or they may partly be owing to the misclassification of the phase. It was because a bin was likely classified into an ice-only containing bin when in reality both ice and liquid were present.

For all cloud types, monthly median values of R_{eff} rarely changed depending on the month (Figures 6, top). Annual mean R_{eff} for liquid droplets was about 6.9±0.8 μm, while those for ice particles were 44.9±1.1 μm and 49.3±1.7 μm in ice and mixed-phase clouds, respectively. On average, liquid droplets were 7 – 8 times smaller than ice particles. Ice particles were larger for mixed-phase clouds than ice clouds because ice particles grow rapidly in mixed-phase conditions by processes referred to as the Bergeron–Findeisen mechanism.

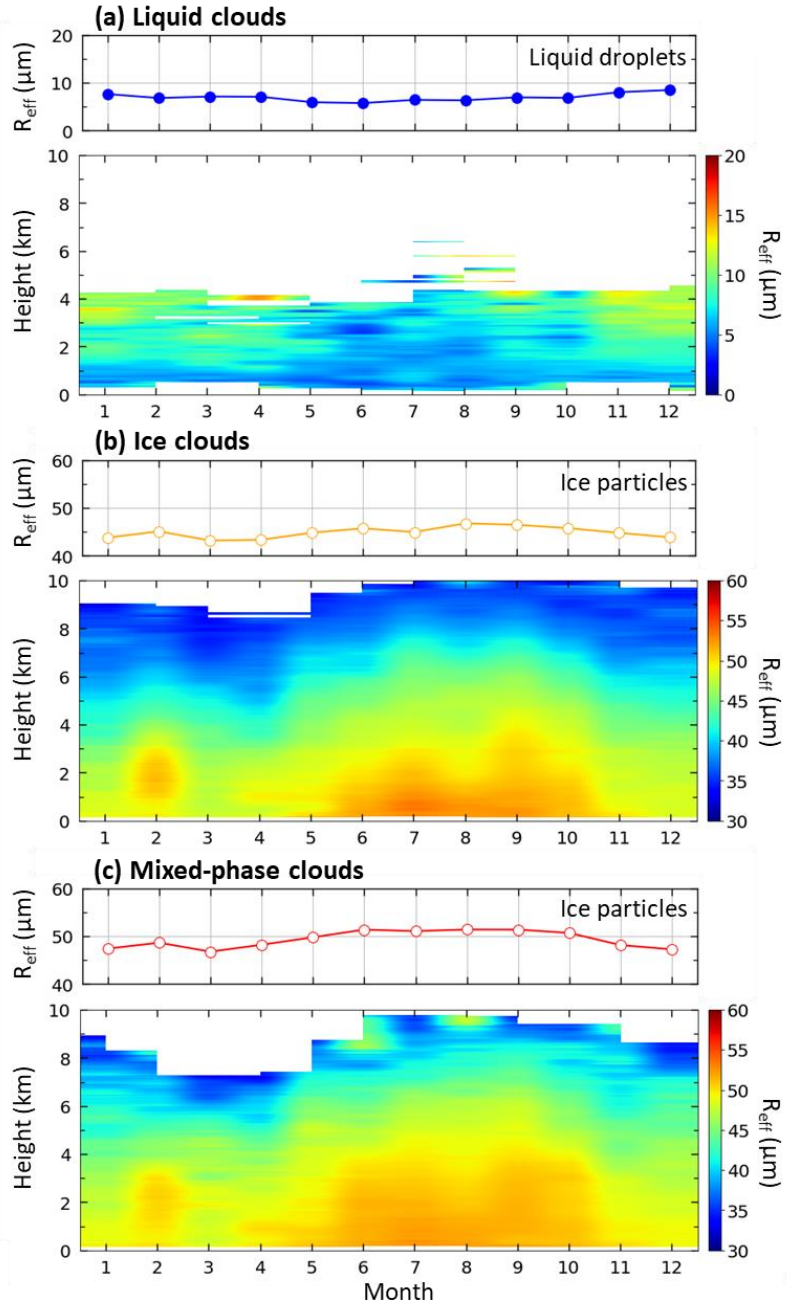

Figure 6. The statistics on R_{eff} for cloud droplets in (a) liquid clouds and R_{eff} for ice particles in (b) ice clouds and (c) mixed-phase clouds from June 2016 to May 2018. The top of each figure shows the monthly variation of median R_{eff} in the vertical profiles. The bottom of each figure is the monthly mean vertical distribution.

3.3 Relationship between air mass origin and microphysical properties of clouds

3.3.1. Warm and cold advections

The variation of cloud properties is associated with atmospheric circulation. The changes in the circulation can alter thermodynamic conditions by increasing (decreasing) tropospheric temperatures and the amount of water vapor. Ny-Ålesund is a region where two types of advection typically intersect. The air masses transported into the site were briefly mentioned in Section 1.1. Advections from the North Atlantic Ocean and the central Arctic were most dominant. It was previously estimated that water content as well as the occurrence of mixed-phase clouds may be affected by factors other than the shortwave radiation, one of which was advection. Thus, investigating the effects of advection is needed to improve understanding of cloud microphysical properties at Ny-Ålesund.

To evaluate the relationship between advection and cloud microphysical properties, we focused on winter (Nov – Feb) when solar radiation was zero. According to previous results, the geometrical and microphysical properties of clouds had seasonality following the cycle of solar radiation. The effect of solar radiation on the clouds is too explicit

to be negligible on a polar day. Therefore, the changes in cloud properties by the advection were clear and the largest in winter. Also, the advection of warm air masses from lower latitudes to Ny-Ålesund increased in winter, contributing to Arctic climate (Maturilli and Kayser, 2017).

Figure 7 shows vertical profiles of temperature in winter during the study period. To decide the warm and cold advection which were distinct at Ny-Ålesund, we analyzed 1h-averaged temperature from MWR for 2-year winter. The bias was calculated by subtracting each monthly mean temperature from hourly mean values at 1450 m. The height was appropriate to explain the large-scale advection. The 5^{th} and 95^{th} of the bias were used as thresholds for case classification. If the bias was higher than the 95^{th} percentile, the hourly mean data was classified into warm cases. Conversely, if the bias is lower than the 5^{th} percentile, it was classified as cold cases.

Using 850 hPa geopotential height from ERA5 reanalysis data, the fields at corresponding hourly cases were averaged. As a result, atmospheric circulation at 850 hPa of warm and cold cases were described in Figure 8. Warm cases with higher temperature bias were related to the air masses coming from the North Atlantic Ocean by south-westerly winds (Figure 8a), while cold cases with lower temperature bias were associated with the air masses transported from the central Arctic

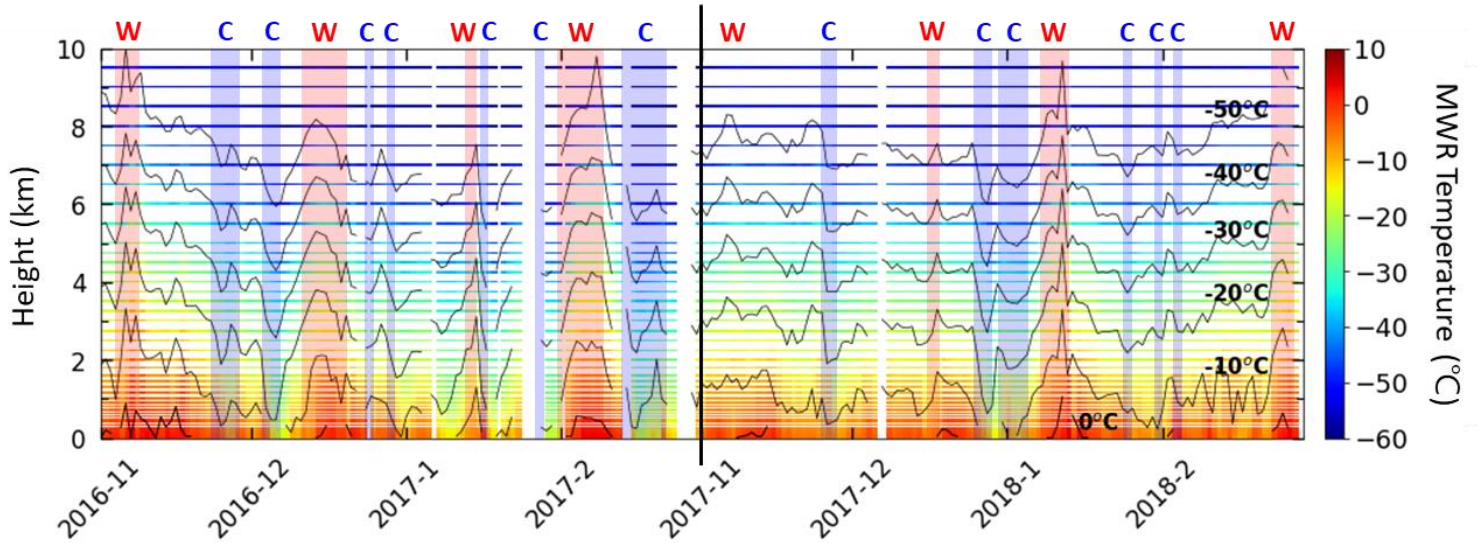

Figure 7. The temperature profiles during 2016 – 2018 winter months (Nov – Feb). Black lines indicate interpolated isotherm. If hourly mean temperature bias at 1450 m is higher than the 95th percentile, the background is filled with red. If the bias is lower than the 5th percentile, the background is filled with blue.

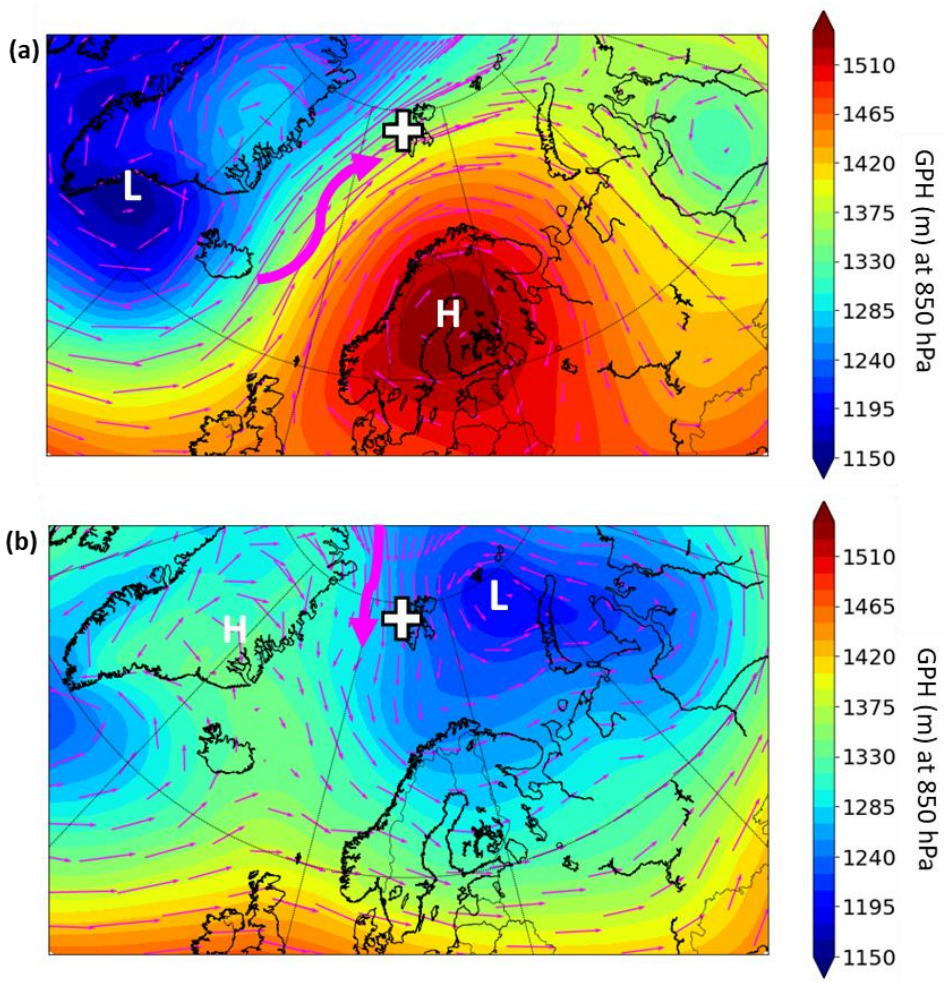

Figure 8. Synthetic geopotential height (GPH) and wind fields at 850 hPa for (a) warm cases and (b) cold cases using ERA5 reanalysis data. The white cross mark indicates the location of Ny-Ålesund. The dominant wind direction around the study region is represented by a pink arrow. 'L' and 'H' denote the low-pressure system (cyclone) and the high-pressure system (anticyclone), respectively.

by northerlies (Figure 8b). From this, we verified that case classification was appropriately performed. Warm and cold cases were, hereafter, defined as warm and cold advection, respectively.

3.3.2. Comparison of cloud microphysical properties

The vertical distributions of microphysical properties were obtained for warm and cold advection classified above. Because the classification was based on the temperature bias, the temperature was higher for all heights under warm advection than cold advection. Note that the mean temperature was lower than 0 °C despite the warm air mass transport since it was winter.

Figure 9 compares the vertical cloud fraction by phase between warm and cold advection. By counting the profiles of each phase, the values were estimated. When warm air masses were transported, clouds occurred during 98 % of the number of profiles classified into warm cases (Figure 9a). Below 3.5 km, mixed-phase cloud occurrence frequency was highest, the maximum value of which was 67 % at 0.7 km. The frequency decreased rapidly with height. On the contrary, ice clouds were present most frequently above 3.5 km. Warm advection also caused liquid clouds, which were normally rare in winter, to occur 6 % below 1 km. On the other hand, cold advection did not contribute to frequent cloud occurrence, the frequency of which was 66 % during cold cases (Figure 9b). In this condition, the occurrence of liquid clouds was close to zero. The cloud fraction of mixed-phase clouds was highest at altitudes

below 1.4 km. The maximum, 25 %, was more than two times lower than that in warm advection. Ice clouds were most frequent above 1.4 km. These results will be valuable to explain the mixed-phase clouds caused by advection, particularly originating from the south.

Differences of microphysical properties, LWC and IWC, between warm and cold advection were displayed in Figure 10. On average, larger LWC and IWC throughout the whole height were caused by intrusions of warm air masses (Figures 10a and 10b). The average LWC at warm advection increased by an order of magnitude than that at cold advection. The average IWC of warm cases was about 10^{-2} to 10^{-1} g cm^{-3}, but that of cold cases was 10^{-3} to 10^{-2} g cm^{-3}, and the former can be observed at higher altitudes. However, R_{eff} of liquid droplets and ice particles were rarely changed by the advection.

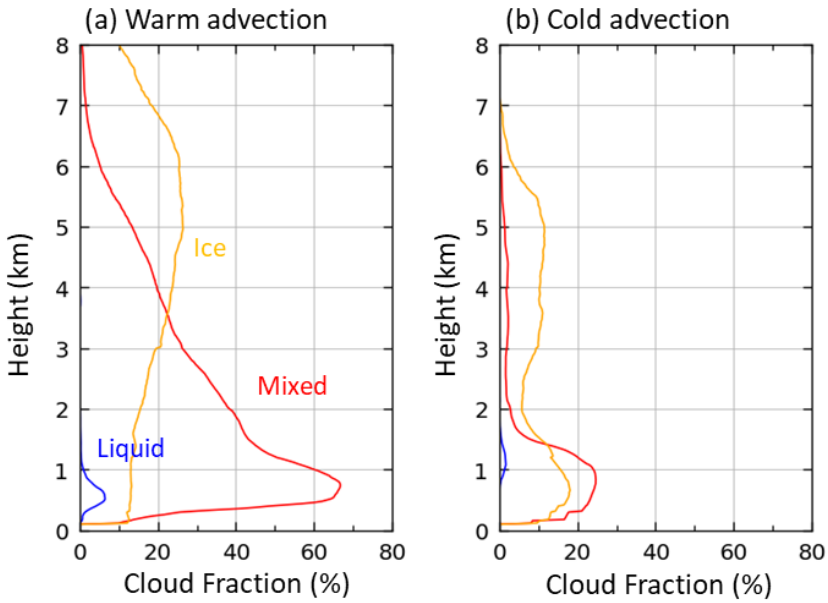

Figure 9. The vertical cloud fraction under (a) warm advection and (b) cold advection for three cloud types (liquid clouds; blue, ice clouds; yellow, mixed-phase clouds; red) in winter (Nov – Feb) 2016 – 2018.

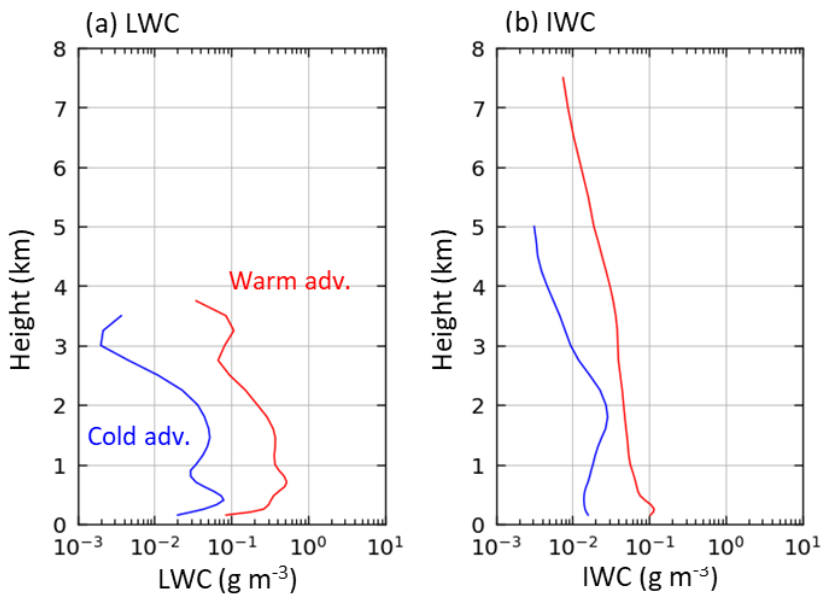

Figure 10. Comparison of (a) LWC and (b) IWC between warm and cold advection in winter (Nov – Feb) 2016 – 2018. Red and blue lines indicate warm and cold advection, respectively.

3.3.3. Effects on the surface longwave (LW) radiation

To confirm the effects of advection on surface LW radiation, a series of cases were selected from warm and cold cases, respectively. Cloud phase profiles were obtained from Cloudnet (Figure 11, top), and surface LW radiation and temperature were taken from Baseline Surface Radiation Network (BSRN; Figure 11, bottom). On 17 December 2016, most of the hours except for 3 hours corresponded to cases of positive temperature biases, warm advection (Figure 11a). Warm advection led to increase in the surface temperature (-2 – 2 °C), resulting in high values of upward LW radiation (287 – 313 W m^{-2}). Thick clouds were observed on this day, and their cloud types were ice or mixed-phase clouds. A large amount of downward LW radiation was emitted ranging from 256 to 315 W m^{-2}. On another day, 29 December 2017 was affected by cold advection in which temperature biases were low (Figure 11b). Surface temperature (-17 – -13 °C) and upward LW radiation (231 – 252 W m^{-2}) decreased compared to the previous warm advection case. Downward LW radiation also decreased significantly into the range from 155 to 242 W m^{-2}, probably due to thin clouds. Through comparison of the two cases, a substantial difference was found in the values of LW radiation by advection.

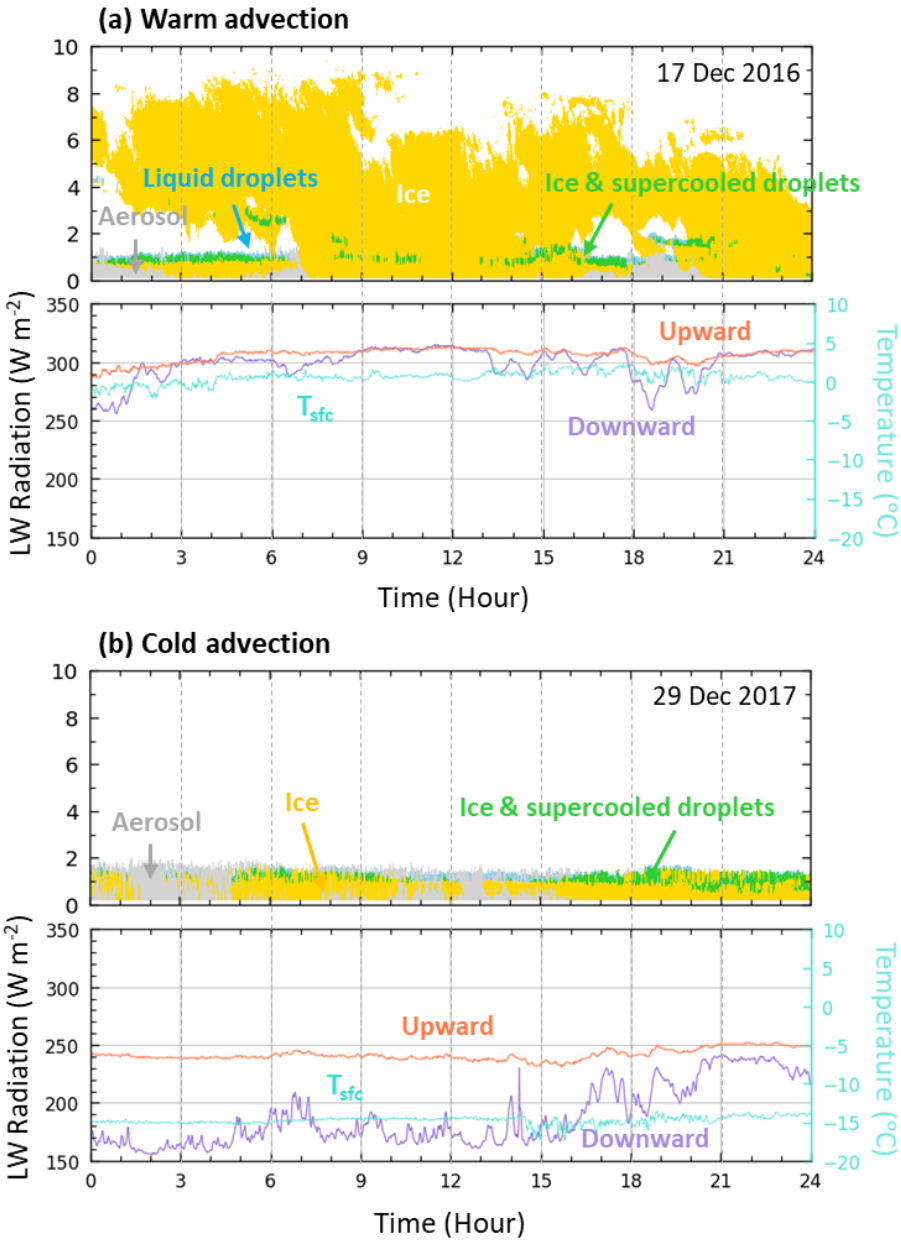

Figure 11. The top of each figure is the phase classification profiles, and the bottom is profiles of both surface longwave radiation (upward; coral, downward; purple) and surface temperature (T_{sfc}; cyan). A series of cases were selected from (a) warm and (b) cold cases, respectively. The selected warm cases are on 17 December 2016, and the cold cases are on 29 December 2017.

Figure 12 represents the frequency distribution of the surface longwave cloud radiative effect (LW CRE) for warm and cold advection. The difference of LW radiation, which was shown in Figure 12, would be affected by cloud properties as well as thermodynamic conditions (temperature and humidity). LW CRE, accordingly, was determined by the difference of LW flux between all-sky and clear-sky to identify only cloud effects. Monthly mean LW fluxes for clear-sky conditions were calculated when the clouds did not occur in the sky. Median downward LW CRE was 145 W m^{-2} higher in warm advection than in cold advection (Figure 12a). Upward LW CRE was also higher in warm advection, but the difference with that of cold advection was low, 83 W m^{-2}, compared to downward LW CRE (Figure 12b). Consequently, total LW CRE subtracted upward from downward LW CRE was weighted to higher values in warm advection (Figure 12c). The median value of warm advection was approximately 1 W m^{-2}, and that of cold advection was 55 W m^{-2}. In other words, cloud properties caused by warm advection can contribute more to increased LW CRE, compared to cold advection.

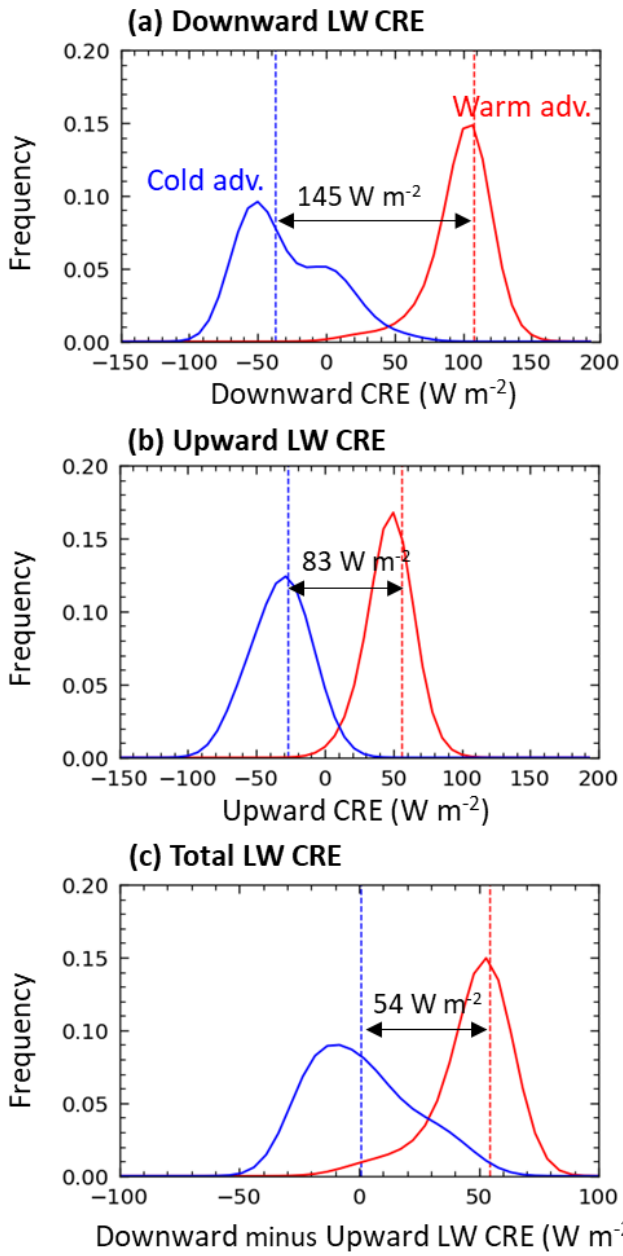

Figure 12. Frequency distribution of (a) downward LW CRE, (b) upward LW CRE, and (c) total LW CRE under warm (red) and cold (blue) advection in winter (Nov – Feb) 2016 – 2018. Total LW CRE is calculated by subtracting upward from downward LW CRE. Red and blue lines indicate warm and cold advection, respectively. Dashed vertical lines are median values of corresponding warm and cold cases.

Chapter 4. Summary

In this study, clouds were investigated at Ny-Ålesund using the ground-based remote sensing observations from June 2016 to May 2018. Based on the target classification product, clouds were classified into three groups, liquid, ice, and mixed-phase clouds. Depending on the types, the monthly variation of cloud geometrical properties (cloud fraction and cloud height), and cloud microphysical properties (LWC, IWC, and R_{eff}) were analyzed. Considering the temperature bias at certain altitudes, air masses transported in winter were classified as warm or cold advection. By comparing the cloud characteristics in each advection, the effects of advection on the clouds were evaluated. Finally, the changes of the surface LW radiation were also estimated.

Three cloud types (liquid, ice, and mixed-phase clouds) showed distinctly different monthly variation of cloud geometrical and microphysical properties. However, they were all associated with the cycle of solar radiation (polar day and polar night). The seasonality of single-phase clouds, liquid and ice clouds, was more clear. Occurrence frequency and LWC of liquid clouds were high at low altitudes in summer and fall, while cloud fraction and IWC of ice clouds increased in winter and spring. On the other hand, mixed-phase clouds showed no clear

seasonality. They were observed predominantly below 2 km throughout the year, with maximum values in the transition months, May and October. The same was true with the variability in the LWC and IWC. The ratio of LWC to IWC in the mixed-phase clouds increased at 1 – 4 km altitudes. From these characteristics of mixed-phase clouds, it was estimated that clouds can be influenced by other factors other than solar radiation.

R_{eff} of cloud droplets and ice particles were also investigated for all cloud types. On average, R_{eff} for ice particles was 7 – 8 times larger than that for cloud droplets. Larger ice particles in summer reflect the growth of ice by aggregation (Shupe et al., 2004) or the misclassification of phase. Ice particles can also grow rapidly in mixed-phase conditions by the Bergeron–Findeisen mechanism.

Cloud fraction was relatively high at Ny-Ålesund, higher even than observation in lower latitudes and the ocean (Shupe et al., 2011a, b). During 78 % of the study period, clouds were observed in this region. The most frequent cloud type was ice clouds, 47 %, followed by mixed-phase clouds (44 %) and ice clouds (15 %). In particular, the ratio of mixed-phase clouds to total clouds in the study region was as high as the ship-based observation, SHEBA. Moreover, they had a larger amount of liquid and ice water than at the other sites with similar latitude (Shupe et al., 2005; Boer et al., 2009). This could be related to the presence of the

surrounding warm North Atlantic Ocean.

Remarkable warm and cold advection were often identified over Ny-Ålesund. The origin of air masses led to changes in cloud microphysical properties in winter. Warm air masses originated from the North Atlantic Ocean by southerlies or south-westerlies. It caused increased LWC, IWC, and more frequent low-level mixed-phase clouds. On the other hand, cold air masses were advected from the central Arctic by northerlies. Under cold advection, the occurrence frequency of ice clouds was high and water contents decreased.

The surface LW radiation was also influenced by warm and cold advection. LW CRE was calculated to identify cloud effects using the monthly mean clear-sky values. As a result, warm advection from the North Atlantic Ocean contributed to the increased downward LW CRE, 145 W m^{-2}, compared to cold advection. Like this, radiative budgets may vary by the atmospheric circulation in the Arctic (Yamanouchi et al., 2018; Park et al., 2015). Thermodynamic conditions and cloud properties, which were affected by advection, can make the variation in LW radiation. In other words, it was proved that radiative properties can depend on cloud geometrical and microphysical properties (Yeo et al., 2018; Dong et al., 2010).

This study serves as the 2-year statistics of cloud microphysical properties which were originally limited to case studies during a few days or months at Ny-Ålesund. It can improve cloud simulation in models by providing more accurate cloud characteristics. The differences in cloud properties depending on the advection are represented as quantitative values, which can emphasize the effects of air circulation. In further works, it is necessary to calculate the CRE through the radiative transfer model to reduce uncertainty. Validation of retrieved cloud microphysical properties used in the study also needs to be done by comparing it with in-situ observations. Although the vertical structure of clouds has begun to be observed using the synergy of radar-lidar, the period is still short. Thus, long-term observations of clouds still need to be performed to accurately investigate their roles in terms of global climate change.

References

Blanchard, Y., Pelon, J., Eloranta, E. W., Moran, K. P., Delanoë, J., and Sèze, G. (2014). A synergistic analysis of cloud cover and vertical distribution from A-Train and ground-based sensors over the high Arctic station EUREKA from 2006 to 2010. Journal of Applied Meteorology and Climatology, 53(11), 2553-2570.

Curry, J. A., Schramm, J. L., Rossow, W. B., and Randall, D. (1996). Overview of Arctic cloud and radiation characteristics. Journal of Climate, 9(8), 1731-1764.

de Boer, G., Eloranta, E. W., and Shupe, M. D. (2009). Arctic mixed-phase stratiform cloud properties from multiple years of surface-based measurements at two high-latitude locations. Journal of the Atmospheric Sciences, 66(9), 2874-2887.

Delanoë, J., Protat, A., Bouniol, D., Heymsfield, A., Bansemer, A., & Brown, P. (2007). The characterization of ice cloud properties from Doppler radar measurements. Journal of applied meteorology and climatology, 46(10), 1682-1698.

Dong, X., Xi, B., Crosby, K., Long, C. N., Stone, R. S., and Shupe, M. D. (2010). A 10-year climatology of Arctic cloud fraction and radiative forcing at Barrow, Alaska. Journal of Geophysical Research: Atmospheres, 115(D17).

Ebell, K., Nomokonova, T., Maturilli, M., and Ritter, C. (2020). Radiative effect of clouds at Ny-Ålesund, Svalbard, as inferred from ground-based remote sensing observations. Journal of Applied

Meteorology and Climatology, 59(1), 3-22.

Frisch, S., Shupe, M., Djalalova, I., Feingold, G., and Poellot, M. (2002). The retrieval of stratus cloud droplet effective radius with cloud radars. Journal of Atmospheric and Oceanic Technology, 19(6), 835-842.

Fukuta, N., and Takahashi, T. (1999). The growth of atmospheric ice crystals: A summary of findings in vertical supercooled cloud tunnel studies. Journal of the Atmospheric Sciences, 56(12), 1963-1979.

Gierens, R., Kneifel, S., Shupe, M. D., Ebell, K., Maturilli, M., and Löhnert, U. (2020). Low-level mixed-phase clouds in a complex Arctic environment. Atmospheric Chemistry and Physics, 20(6), 3459-3481.

Goosse, H., Kay, J. E., Armour, K. C., Bodas-Salcedo, A., Chepfer, H., Docquier, D., Jonko, A., Kushner, P. J., Lecomte, O., Massonnet, F., Park, H. S., Pithan, F., Svensson, G., and Vancoppenolle, M. (2018). Quantifying climate feedbacks in polar regions. Nature communications, 9(1), 1-13.

Hogan, R. J., and O'Connor, E. J. (2004). Facilitating cloud radar and lidar algorithms: the Cloudnet Instrument Synergy/Target Categorization product. Cloudnet documentation.

Hogan, R. J., Mittermaier, M. P., and Illingworth, A. J. (2006). The retrieval of ice water content from radar reflectivity factor and temperature and its use in evaluating a mesoscale model. Journal of Applied Meteorology and Climatology, 45(2), 301-317.

Illingworth, A. J., Hogan, R. J., O'connor, E. J., Bouniol, D., Brooks, M. E.,

Delanoë, J., Donovan, D. P., Eastment, J. D., Gaussiat, N., Goddard, J. W. F., Haeffelin, M., Klein Baltink, H., Krasnov, O. A., Pelon, J., Piriou, J. -M., Protat, A., Russchenberg, H. W. J., Seifert, A., Tompkins, A. M., van Zadelhoff, G. –J., Vinit, F., Willén, U., Wilson, D. R., and Wrench, C. L. (2007). Cloudnet: Continuous evaluation of cloud profiles in seven operational models using ground-based observations. Bulletin of the American Meteorological Society, 88(6), 883-898.

Kim, B. M., Hong, J. Y., Jun, S. Y., Zhang, X., Kwon, H., Kim, S. J., Kim, J. H., Kim, S. W., and Kim, H. K. (2017). Major cause of unprecedented Arctic warming in January 2016: Critical role of an Atlantic windstorm. Scientific reports, 7, 40051.

Küchler, N., Kneifel, S., Löhnert, U., Kollias, P., Czekala, H., and Rose, T. (2017). A W-Band radar–radiometer system for accurate and continuous monitoring of clouds and precipitation. Journal of Atmospheric and Oceanic Technology, 34(11), 2375-2392.

Liu, Y., Shupe, M. D., Wang, Z., and Mace, G. (2017). Cloud vertical distribution from combined surface and space radar-lidar observations at two Arctic atmospheric observatories. Atmospheric Chemistry and Physics (Online), 17(9).

Nomokonova, T., Ebell, K., Löhnert, U., Maturilli, M., Ritter, C., and O'Connor, E. (2019). Statistics on clouds and their relation to thermodynamic conditions at Ny-Ålesund using ground-based sensor synergy. Atmospheric Chemistry and Physics, 19, 4105-4126.

Maturilli, M., and Kayser, M. (2017). Arctic warming, moisture increase and circulation changes observed in the Ny-Ålesund homogenized radiosonde record. Theoretical and Applied Climatology, 130(1-2), 1-17.

Maturilli, M., and Ebell, K. (2018). Twenty-five years of cloud base height measurements by ceilometer in Ny-Ålesund, Svalbard. Earth System Science Data, 10, 1451-1456.

Miles, N. L., Verlinde, J., and Clothiaux, E. E. (2000). Cloud droplet size distributions in low-level stratiform clouds. Journal of the atmospheric sciences, 57(2), 295-311.

Mioche, G., Jourdan, O., Ceccaldi, M., and Delanoë, J. (2015). Variability of mixed-phase clouds in the Arctic with a focus on the Svalbard region: a study based on spaceborne active remote sensing. Atmospheric Chemistry and Physics, 15(5), 2445-2461.

Park, D. S. R., Lee, S., and Feldstein, S. B. (2015). Attribution of the recent winter sea ice decline over the Atlantic sector of the Arctic Ocean. Journal of Climate, 28(10), 4027-4033.

Rose, T., Crewell, S., Löhnert, U., and Simmer, C. (2005). A network suitable microwave radiometer for operational monitoring of the cloudy atmosphere. Atmospheric Research, 75(3), 183-200.

Serreze, M. C., Barrett, A. P., Stroeve, J. C., Kindig, D. N., and Holland, M. M. (2009). The emergence of surface-based Arctic amplification. The Cryosphere, 3(1), 11.

Serreze, M. C., Barrett, A. P., and Cassano, J. J. (2011). Circulation and surface controls on the lower tropospheric air temperature field of

the Arctic. Journal of Geophysical Research: Atmospheres, 116(D7).

Shupe, M. D., and Intrieri, J. M. (2004). Cloud radiative forcing of the Arctic surface: The influence of cloud properties, surface albedo, and solar zenith angle. Journal of Climate, 17(3), 616-628.

Shupe, M. D., Uttal, T., and Matrosov, S. Y. (2005). Arctic cloud microphysics retrievals from surface-based remote sensors at SHEBA. Journal of Applied Meteorology, 44(10), 1544-1562.

Shupe, M. D., Walden, V. P., Eloranta, E., Uttal, T., Campbell, J. R., Starkweather, S. M., and Shiobara, M. (2011a). Clouds at Arctic atmospheric observatories. Part I: Occurrence and macrophysical properties. Journal of Applied Meteorology and Climatology, 50(3), 626-644.

Shupe, M. D. (2011b). Clouds at Arctic atmospheric observatories. Part II: Thermodynamic phase characteristics. Journal of Applied Meteorology and Climatology, 50(3), 645-661.

Twomey, S. (1977). The influence of pollution on the shortwave albedo of clouds. Journal of the Atmospheric Sciences, 34(7), 1149-1152.

Yamanouchi, T. (2019). Arctic warming by cloud radiation enhanced by moist air intrusion observed at Ny-Ålesund, Svalbard. Polar Science, 21, 110-116.

Yeo, H., Park, S. J., Kim, B. M., Shiobara, M., Kim, S. W., Kwon, H., Kim J. H., Jeong, J. H., Park, S. S., and Choi, T. (2018). The observed relationship of cloud to surface longwave radiation and air temperature at Ny-Ålesund, Svalbard. Tellus B: Chemical and Physical Meteorology, 70(1), 1-10.

국문 초록

니알슨 지역 지상 원격 관측자료를 활용한 북극 구름의 미세물리 특성 연구

조 연 수

지구환경과학부

서울대학교 대학원

본 연구에서는 스발바드 제도에 위치한 니알슨에서 발생하는 구름의 기하학적 그리고 미세물리 특성들을 2016년 6월부터 2018년 5월까지의 지상 원격 관측(구름 레이더, 운고계, 마이크로웨이브 라디오미터)을 이용하여 조사하였다. 구름 유형(액체, 얼음, 혼합상 구름)에 따른 구름 특성들의 월 변동성을 분석하고, 그들의 이류와의 관계를 평가했다. 분석 기간 동안, 니알슨의 총 구름 발생 비율은 78%였고, 얼음 구름(44%)이 가장 많이 발생했다. 구름 발생 비율과 구름의 수분 함량(액체 수분 함량, 얼음 수분 함량)의 경우, 액체 구름에서는 여름/가을에 얼음 구름에서는 겨울/봄에 높은 값이 나타났다. 그에 반해, 혼합상 구름의 특성들은 뚜렷한 월 변동성을 보이지 않았다. 구름 미세물리 특성에 대한 온난 이류와 한랭 이류의 영향을 겨울에 한정하여 확인하였다. 결과는 북대서양으로부터 이동해온 온난

이류 하에서, 하층 혼합상 구름은 2배 이상 더 빈번하게 발생했고 액체 수분 함량/얼음 수분 함량 또한 10배 정도 증가했다는 것을 보여주었다. 더 나아가, 온난 이류에 의해 야기된 구름 미세물리 특성들은 한랭 이류보다 145 W m^{-2} 만큼 더 높은 하향 장파 구름 복사 효과에 기여하여, 지표면 가열을 초래하였다.

주 요 어 : 북극 구름, 지상 원격 관측, 구름 미세물리 특성, 이류, 장파 구름 복사 효과

학 번 : 2018-27016